Laser induced sponge-like Si in Si-rich oxides for photovoltaics

Article *in* Optics Express · October 2013

DOI: 10.1364/OE.21.024368 · Source: PubMed

5 authors, including:

Karl-Heinz Heinig
Helmholtz-Zentrum Dresden-Rossendorf
144 PUBLICATIONS **2,244** CITATIONS

SEE PROFILE

Laser induced sponge-like Si in Si-rich oxides for photovoltaics

S. Gundogdu,[1] E. Sungur Ozen,[1*] R. Hübner,[2] K. H. Heinig,[2] and A. Aydinli[1]

[1]*Department of Physics, Bilkent University, 06800, Ankara, Turkey*
[2]*Helmholtz-Zentrum Dresden-Rossendorf, PO Box 510119, 01314 Dresden, Germany*
[*]*sungur@fen.bilkent.edu.tr*

Abstract: We show that a sponge-like structure of interconnected Si nanowires embedded in a dielectric matrix can be obtained by laser annealing of silicon rich oxides (SRO). Due to quantum confinement, the large bandgap displayed by these percolated nanostructures can be utilized as a tandem stage in 3rd generation thin-film solar cells. Well passivated by the SiO_2 dielectric matrix, they are expected to overcome the difficulty of carrier separation encountered in the case of isolated crystalline quantum dots. In this study PECVD grown SRO were irradiated by a cw Ar^+ laser. Raman spectroscopy has been used to assess the crystallinity of the Si nanostructures and thus to optimize the annealing conditions as dwell times and power densities. In addition, Si plasmon imaging in the transmission electron microscope was applied to identify the sponge-like structure of phase-separated silicon.

OCIS codes: (350.3390) Laser materials processing; (160.4236) Nanomaterials; (310.6845) Thin film devices and applications.

References and links

1. A. Polman and H. A. Atwater, "Photonic design principles for ultrahigh-efficiency photovoltaics," Nat. Mater. **11**(3), 174–177 (2012).
2. G. Conibeer, "Third-generation photovoltaics," Mater. Today **10**(11), 42–50 (2007).
3. E. G. Barbagiovanni, D. J. Lockwood, P. J. Simpson, and L. V. Goncharova, "Quantum confinement in Si and Ge nanostructures," J. Appl. Phys. **111**(3), 034307 (2012).
4. J. Carrillo-López, J. A. Luna-López, I. Vivaldo-De la Cruz, M. Aceves-Mijares, A. Morales-Sanchez, and G. García-Salgado, "UV enhancement of silicon solar cells using thin SRO films," Sol. Energy Mater. Sol. Cells **100**, 39–42 (2012).
5. G. Conibeer, M. A. Green, R. Corkish, Y.-H. Cho, E.-C. Cho, and C.-W. Jiang, "Silicon nanostructures for third generation photovoltaic solar cells," Thin Solid Films **654**, 511–512 (2005).
6. N. Tomozeiu, "Silicon oxide (SiOx, 0<x<2): a challenging material for optoelectronics," Optoelectronics - Materials and Techniques, Prof. P. Predeep (Ed.), (2011).
7. B.-H. Kim, C.-H. Cho, T.-W. Kim, N.-M. Park, G. Y. Sung, and S.-J. Park, "Photoluminescence of silicon quantum dots in silicon nitride grown by NH3 and SiH4," Appl. Phys. Lett. **86**(9), 091908 (2005).
8. Z. Wan, S. Huang, M. A. Green, and G. Conibeer, "Rapid thermal annealing and crystallization mechanism study of Si-NCs in SiC matrix," Nanoscale Res. Lett. **6**, 129 (2011).
9. M. D. Kelzenberg, M. C. Putnam, D. B. Turner-Evans, N. S. Lewis, and H. A. Atwater, "Predicted efficiency of Si wire array solar cells," Appl. Phys. Lett. **93**, 032112 (2008).
10. B.-R. Huang, Y.-K. Yang, T.-C. Lin, and W.-L. Yang, "A simple and low-cost technique for silicon nanowire arrays based solar cells," Sol. Energy Mater. Sol. Cells **98**, 357–362 (2012).
11. L. Yu, B. O'Donnell, P.-J. Alet, and P. R. Cabarrocas, "All-in-situ fabrication and characterization of silicon nanowires on TCO/glass substrates for photovoltaic application," Sol. Energy Mater. Sol. Cells **94**(11), 1855–1859 (2010).
12. B. Tian, X. Zheng, T. J. Kempa, Y. Fang, N. Yu, G. Yu, J. Huang, and C. M. Lieber, "Coaxial silicon nanowires as solar cells and nanoelectronic power sources," Nature **449**(7164), 885–889 (2007).
13. L. Tsakalakos, J. Balch, J. Fronheiser, B. A. Korevaar, O. Sulima, and J. Rand, "Silicon nanowire solar cells," Appl. Phys. Lett. **91**(23), 233117 (2007).
14. M. D. Kelzenberg, D. B. Turner-Evans, B. M. Kayes, M. A. Filler, M. C. Putnam, N. S. Lewis, and H. A. Atwater, "Photovoltaic Measurements in Single-Nanowire Silicon Solar Cells," Nano Lett. **8**(2), 710–714 (2008).
15. B. O'Donnell, L. Yu, M. Foldyna, and P. R. Cabarrocas, "Silicon nanowire solar cells grown by PECVD," J. Non-Cryst. Solids **358**(17), 2299–2302 (2012).

#194332 - $15.00 USD Received 22 Jul 2013; revised 20 Sep 2013; accepted 24 Sep 2013; published 4 Oct 2013

16. T. J. Kempa, B. Tian, D. R. Kim, J. Hu, X. Zheng, and C. M. Lieber, "Single and Tandem Axial p-i-n Nanowire Photovoltaic Devices," Nano Lett. **8**(10), 3456–3460 (2008).
17. J. Cho, B. O'Donnell, L. Yu, K.-H. Kim, I. Ngo, and P. R. Cabarrocas, "Sn-catalyzed silicon nanowire solar cells with 4.9% efficiency grown on glass," Prog. Photovolt. Res. Appl. **21**(1), 77–81 (2013).
18. P. Cuony, D. T. L. Alexander, I. Perez-Wurfl, M. Despeisse, G. Bugnon, M. Boccard, T. Söderström, A. Hessler-Wyser, C. Hébert, and C. Ballif, "Silicon filaments in silicon oxide for next-generation photovoltaics," Adv. Mater. **24**(9), 1182–1186 (2012).
19. B. Hinds, Wang, F. Wolfe, D. Hinkle, and G. Lucovsky, "Investigation of postoxidation thermal treatments of Si/SiO2 interface in relationship to the kinetics of amorphous Si suboxide decomposition," J. Vac. Sci. Technol. B **16**, 2171–2177 (1998).
20. D. Riabinina, C. Durand, J. Margot, M. Chaker, G. A. Botton, and F. Rosei, "Nucleation and growth of Si nanocrystals in an amorphous SiO2 matrix," Phys. Rev. B **74**(7), 075334 (2006).
21. R. A. R. Oliveira, M. Ribeiro, I. Pereyra, and M. I. Alayo, "Silicon clusters in PECVD silicon-rich SiOxNy," Mater. Charact. **50**(2-3), 161–166 (2003).
22. J. J. van Hapert, A. M. Vredenberg, E. E. van Faassen, N. Tomozeiu, W. M. Arnoldbik, and F. H. P. M. Habraken, "Role of spinodal decomposition in the structure of SiOx," Phys. Rev. B **69**(24), 245202 (2004).
23. T. Muller, K.-H. Heinig, W. Moller, C. Bonafos, H. Coffin, N. Cherkashin, G. Ben Assayag, S. Schamm, G. Zanchi, A. Claverie, M. Tence, and C. Colliex, "Multi-dot floating-gates for nonvolatile semiconductor memories: Their ion beam synthesis and morphology," Appl. Phys. Lett. **85**(12), 2373–2376 (2004).
24. T. Muller, K.-H. Heinig, and W. Moller, "Size and location control of Si nanocrystals at ion beam synthesis in thin SiO2 films," Appl. Phys. Lett. **81**(16), 3049–3052 (2002).
25. A. Janotta, Y. Dikce, M. Schmidt, C. Eisele, M. Stutzmann, M. Luysberg, and L. Houben, "Light-induced modification of a-SiO[sub x] II: Laser crystallization," J. Appl. Phys. **95**(8), 4060–4069 (2004).
26. L. Khriachtchev, T. Nikitin, M. Rasanen, A. Domanskaya, S. Boninelli, F. Iacona, A. Engdahl, J. Juhanoja, and S. Novikov, "Continuous-wave laser annealing of Si-rich oxide: A microscopic picture of macroscopic Si[Single Bond]SiO2 phase separation," J. Appl. Phys. **108**(12), 124301 (2010).
27. L. Khriachtchev, "Optical and structural properties of silicon nanocrystals and laser-induced thermal effects'," J. Electrochem. Soc. **159**(1), K21–K26 (2012).
28. I. Balberg, E. Savir, J. Jedrzejewski, A. G. Nassiopoulou, and S. Gardelis, "Fundamental tansport processes in ensembles of silicon quantum dots," Phys. Rev. B **75**(23), 235329 (2007).
29. R. Elliman, "The synthesis of silicon nanocrystals by ion implantation" *Silicon Nanocrystals: Fundamentals, Synthesis and Applications*, Lorenzo Pavesi and Rasit Turan,eds. (Wiley, 2010), Chap. 9.
30. N. P. Barradas, C. Jeynes, and R. P. Webb, "Simulated annealing analysis of rutherford backscattering data," Appl. Phys. Lett. **71**(2), 291–293 (1997).
31. S. P. Singh, P. Srivastava, S. Ghosh, S. A. Khan, and G. Vijaya Prakash, "Phase stabilization by rapid thermal annealing in amorphous hydrogenated silicon nitride film," J. Phys. Condens. Matter **21**(9), 095010 (2009).
32. G. Franzò, M. Miritello, S. Boninelli, R. Lo Savio, M. G. Grimaldi, F. Priolo, F. Iacona, G. Nicotra, C. Spinella, and S. Coffa, "Microstructural evolution of SiOx films and its effect on the luminescence of Si nanoclusters," J. Appl. Phys. **104**(9), 094306 (2008).
33. D. Barba, F. Martin, and G. G. Ross, "Evidence of localized amorphous silicon clustering from Raman depth-probing of silicon nanocrystals in fused silica," Nanotechnology **19**(11), 115707 (2008).
34. S. Schamm, C. Bonafos, H. Coffin, N. Cherkashin, M. Carrada, G. Ben Assayag, A. Claverie, M. Tencé, and C. Colliex, "Imaging Si nanoparticles embedded in SiO_2 layers by (S)TEM-EELS," Ultramicroscopy **108**(4), 346–357 (2008).
35. Y. Ritz, H. Stegmann, H.-J. Engelmann, and E. Zschech, "Target preparation of samples for 3D-TEM using micromanipulators," Prakt. Metallogr. **41**, 180–189 (2004).
36. C. M. M. Denisse, K. Z. Troost, J. B. Oude Elferink, F. H. P. M. Habraken, and M. Hendriks, "Plasma-enhanced growth and composition of silicon oxynitride films," J. Appl. Phys. **60**(7), 2536–2542 (1986).
37. F. Iacona, C. Bongiorno, C. Spinella, S. Boninelli, and F. Priolo, "Formation and evolution of luminescent Si nanoclusters produced by thermal annealing of SiOx films," J. Appl. Phys. **95**(7), 3723–3733 (2004).

1. Introduction

Silicon based solar cells have been studied extensively due to their low cost, however, the efficiency of a single junction solar cell is relatively small and is restricted to the Shockley-Queisser. To increase the efficiency, multi-junction approaches can be used [1, 2]. One strategy is the implementation of tandem connection of two or more solar cell junctions with differing band gaps to obtain large spectral coverage. Differing band gaps can be obtained either by utilizing alloys of silicon such as SiGe or by band gap engineering silicon itself. The latter requires the formation of Si nanocrystals of a few nm in dimension which result in wider band gaps due to the quantum confinement effects. The magnitude of the bandgap depends on nanocrystal size, opening up for nanocrystal sizes below 5 nm and theoretically reaching 3.0 eV for nanocrystal sizes of ~1nm [3]. Based on this effect, Si nanostructure tandem photovoltaic cells have been proposed in the past [2, 4, 5]. Bandgap engineering has

#194332 - $15.00 USD Received 22 Jul 2013; revised 20 Sep 2013; accepted 24 Sep 2013; published 4 Oct 2013

been tried in quantum dots of Si sandwiched between layers of a dielectrics such as SiO_2 [4–6], Si_3N_4 [5, 7] or SiC [5, 8]. However, charges created in dielectric embedded Si nanocrystals require either tunneling or impact ionization in order to extract useful current from the solar cell before carrier recombination. Both processes require precise positioning of Si nanocrystals within the dielectrics with oxide barriers of a few nanometers, which is a severe challenge. The replacement of Si nanocrystals with ordered arrays of Si nanowires can be a solution to overcome the difficulty of charge transport. Being naturally passivated with low density of defects, these structures should have good electrical conduction. Si nanowire based solar cells were realized in the past in order to enhance absorption and decrease cost [9–17]. In these works, silicon nanowires were formed on silicon wafers by various methods. Despite exotic approaches such as single nanowire solar cells [14], coaxial nanowire pn junctions [12, 16], vapor liquid solid (VLS) growth of Si and other semiconductor nanowires for solar cells on a variety of substrates [13, 17], a significant enhancement of solar cell performance is still lacking. Furthermore, fabrication of ordered arrays of nanowires can be difficult and costly for large scale production. Alternatively, a sponge-like structure created by the precipitation of excess Si in an oxide matrix in the form of percolated randomly oriented nanowires can be considered. Spinodal decomposition of metastable Si-rich oxides is a promising synthesis process for the formation of crystalline Si sponge-like structures. These structures can be used in a multi-junction approach, to improving the single bandgap silicon solar cell efficiency with the incorporation of larger bandgap nanocrystalline Si structures onto the solar cells, allowing a larger spectral coverage. Recently, randomly oriented nanowire approach has been tried by growing silicon filaments in SiO_2 using plasma enhanced chemical vapor deposition (PECVD). In this approach, a tandem solar cell with microcrystalline Si and amorphous Si (a-Si) layers containing Si filaments sandwiched between ZnO layers was fabricated and stabilized conversion efficiency of 11.5% was reached [18].

In this report, we propose an alternative method for obtaining crystalline Si sponge-like nanowires in SiO_2 by laser processing of silicon rich oxide (SRO) thin films to be used as a tandem cell element. Upon laser annealing, SRO films separate into two phases following the equation: $SiO_x \rightarrow 0.5\ SiO_2 + (1 - 0.5\ x)\ Si$, as has been observed in furnace annealing [6, 19–21]. The phase separation is a consequence of nucleation followed by growth, and Ostwald ripening of Si precipitates or, at higher Si concentrations, of spinodal decomposition [20, 22, 23]. Different mechanisms will have different impact on the final structure of the Si precipitates. In fact, in the case of SRO formed by ion implanted Si in SiO_2 matrix, Monte Carlo simulation of the thermally activated precipitation show that the structure of the phase separated Si depends on the fluence of the Si ion beam that was used during ion implantation [23]. For low fluences (low excess Si), individual spheroid Si nanoparticles were obtained, while for high fluences (high excess Si), Si nanoparticles formed an interconnected network. This dependence was also shown experimentally in a later work [24]. However, this method of both ion beam synthesis and thermal processing of the whole solar cell with its high thermal budget, is costly. Laser processing, on the other hand, heats the film surface only and gives the further flexibility of "writing" on selected areas. Continuous and pulsed laser processing of SRO thin films were shown to produce Si nanocrystals in SiO_2 [25–27]. In these works, individual nanocrystals were obtained. Despite the intensity of interest in individual Si nanocrystals for many applications, little has been done to study interconnected nanocrystalline Si in an oxide matrix. Depending on the silicon content of the SRO films, individual nanocrystals or a sponge-like interconnected crystalline Si structures can form in SiO_2. Photoluminescence or electrical transport studies in nanocrystalline Si formed upon phase separation into SiO_2 suggest that the films with x = O/Si ratio close to 1 results in a percolated structure [23, 24, 28, 29]. Here, we demonstrate the formation of sponge-like Si in PECVD grown SRO films by cw laser annealing. This structure is particularly interesting due to the nearly perfect passivation in a SiO_2 matrix which makes it ideal for carrier transport in thin film solar cells.

#194332 - $15.00 USD Received 22 Jul 2013; revised 20 Sep 2013; accepted 24 Sep 2013; published 4 Oct 2013

2. Experimental

A commercial radial flow capacitively coupled parallel-plate PECVD reactor operating at 13.56 MHz radio frequency was used to deposit about 300 nm thick films with hydrogen diluted silane (2% SiH_4 in H_2) and CO_2 gases. The reactor chamber pressure was set at 500 mTorr, the substrate temperature at 250 °C and the rf power at 50 W. To obtain samples with different compositions silane flow rate was fixed at 350 sccm and the CO_2 rate was varied between 10 and 50 sccm. Elastic Recoil Detection Analysis (ERDA) was used to determine elemental composition of the films. The measurements were performed using a 35 MeV Cl^{7+} ion beam. All ERD spectra were fitted simultaneously using the program NDF [30].

Laser processing of the films was done by focusing the 488 nm line of a cw Ar^+ laser in an inverted microscope. The focused spot size was measured using a silicon photodetector by razor-edge scanning and found to be 5 ± 1 μm. The sample was moved on a computer controlled XY stage to form laser irradiated lines on the surface of the films. For different given power densities many line scans were made at different scan speeds and the precipitation and subsequent crystallization of the silicon was checked by Raman spectroscopy. Raman scattering experiments were performed using the same setup while collecting the scattered light with a high resolution monochromator and CCD camera system to determine both the presence and the crystallinity of the phase separated Si. A typical example of a scanned line on a thin SRO film deposited on a quartz substrate is given in the optical microscope image, Fig. 1. The surface depth profile across the scanned line and Raman signal amplitude obtained at various points along the line perpendicular to the laser scanned line are presented superimposed on the optical image. Surface profile indicates densification (~10%) of the SRO film in scanned regions as is expected in PECVD grown SRO films, amplified due, in particular, to hydrogen out-diffusion [31]. Raman spectrum of the annealed zone includes the signal from the quartz substrate as well as contributions from remaining or clustered amorphous Si characterized by a broad peak at 480 cm^{-1} and a peak at 518 cm^{-1} corresponding to crystalline Si. It is known in the literature that some of the Si can cluster in the amorphous form upon phase separation [32, 33]. The down shift of the crystalline peak from the bulk c-Si peak at ~520 cm^{-1} is due to the nanoparticle nature of the aggregated silicon.

To characterize the microstructure as well as the morphology of laser-annealed SRO films, transmission electron microscopy analyses were performed. To avoid possible charging effects during TEM lamellae target preparation using the focused ion beam technique as well as during further TEM analysis, SRO films were prepared on Si wafers. This, in turn, results in Raman scattering from the substrate in addition to scattering from Si nanocrystals from laser annealed SRO films, complicating the analysis of SRO films on silicon wafers. To eliminate the substrate contribution, the polarization selection rules were used to discriminate against Raman signals from the Si substrate. In the as-grown SRO region of the sample, the polarization of the incident laser beam in the nearly backscattering configuration was set with a Glan-Thomson polarization rotator while the polarization of the scattered light was selected with a polarizer at the entrance slits of the monochromator until the Raman scattering from the Si substrate was totally suppressed. Then, the sample was translated to measure the Raman spectrum form the Si nanostructures in the annealed region of the SRO film. In this case, the remaining signal corresponds to the signal from the randomly oriented crystalline nanostructures, as they don't have any preferential orientation.

#194332 - $15.00 USD Received 22 Jul 2013; revised 20 Sep 2013; accepted 24 Sep 2013; published 4 Oct 2013

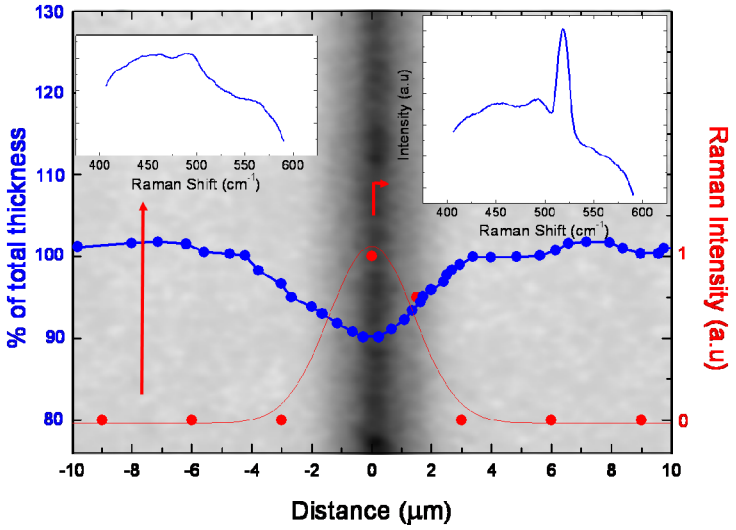

Fig. 1. Optical microscope image of a laser scanned line on a SRO thin film on quartz substrate with the surface depth profile data and normalized Raman peak intensity of selected spots superimposed (the red curve is a guide for the eye).

To characterize the formation of the Si nanostructures, laser-annealed samples were analyzed using high-resolution transmission electron microscopy (HRTEM) and energy-filtered transmission electron microscopy (EFTEM) employing an image-corrected FEI Titan 80-300 microscope equipped with a Gatan Imaging Filter 863. In particular, HRTEM was used to visualize Bragg-oriented Si nanocrystals larger than a minimum size. Applying energy filtering, chemical sensitivity is added to the TEM analysis. Consequently, nanoparticles independent of their crystalline structure, i.e. amorphous as well as crystalline nanostructures, can be characterized. In particular, valence-band plasmon energy-loss imaging is an appropriate approach, since the Si plasmon peak is, except the zero-loss peak, the most intense feature in the electron energy-loss spectrum. Located at an energy loss of about 17 eV, it has a narrow energy distribution of a few eV, and thus, allows distinguishing the Si phase from the SiO_2 compound [34]. TEM sample preparation was done by in situ lift-out applying a Kleindiek micromanipulator in a Zeiss NVision 40 Focused Ion Beam device [35].

3. Results

Following the ERD analysis, films were found to have x = O/Si ratios increasing with CO_2 flow rate and in the range of 0.47 to 0.97. The samples present small amounts of nitrogen (< 2%), carbon (< 4%), and hydrogen (~10%). It is well known that PECVD-grown SRO layers incorporate hydrogen [36]. Assuming that hydrogen binds in large parts to oxygen and nitrogen and that nitrogen and carbon behave similarly to oxygen in the phase separation process, we considered samples with x' = (O + N + C)/Si ~1 for this study. In particular, SRO films with the chemical formula $SiO_{0.79}N_{0.04}C_{0.08}H_{0.18}$, i.e. with x' = 0.91, were chosen for the analyses. Figure 2 (a) shows an optical microscope image of a laser-annealed square of 500 x 500 μm^2 formed by laser scanning lines 1 μm apart. Figure 2 (b) is a corresponding SEM image of the scanned zone showing that the scanned surface becomes rough on a microscopic scale. This can be attributed to the out-diffusion of hydrogen during laser annealing. The Raman signals in Fig. 3 were taken from the as-grown and the annealed zones under forbidden polarization conditions. The peak at around 518 cm^{-1} is characteristic of the nanocrystalline Si TO Raman mode and gives evidence of the presence of crystalline nanostructures.

#194332 - $15.00 USD Received 22 Jul 2013; revised 20 Sep 2013; accepted 24 Sep 2013; published 4 Oct 2013

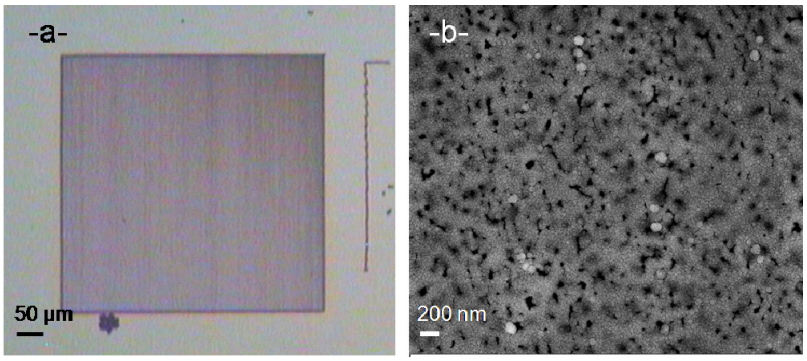

Fig. 2. a) Optical microscope image of a laser-scanned square on a $SiO_{0.79}N_{0.04}C_{0.08}H_{0.18}$ sample (laser power density 500 kW/cm^2, scan speed 0.05 mm/s), b) SEM image of the scanned zone.

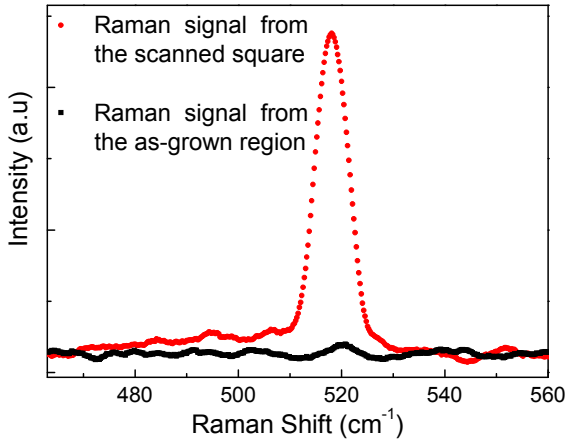

Fig. 3. Raman signal from the as-grown region and the annealed square on the $SiO_{0.79}N_{0.04}C_{0.08}H_{0.18}$ sample. Polarization selection method has been used to eliminate the signal from the Si substrate.

TEM technique was used to observe these structures. Figure 4 (a) shows a cross-sectional Si plasmon EFTEM image of the SRO film / Si substrate region of the laser-annealed area. A sponge-like structure corresponding to precipitated Si (white) inside the oxide matrix (black) can be identified at a tunneling distance of a few nanometers from the interface. The interconnected Si nanostructure of the network is seen best in Fig. 4 (b), a Si plasmon image recorded at higher magnification with the field of view marked by a square in Fig. 4 (a). Near the SRO-substrate interface the diameters of the wires are in the order of 3 nm. We can observe a size gradient with Si aggregates becoming larger as the distance from the SRO-substrate interface increases. This size gradient may be due to a temperature gradient generated by a relatively cold SRO-substrate interface resulting from the high thermal conductivity of the Si substrate. We note the absence of nanocrystals in the top 80 nm of the SRO film (not shown here) and suggest that this is mainly due to oxidation during irradiation. Figure 4 (c) is the zero-loss filtered image corresponding to the same field of view as in Fig. 4 (b), and it demonstrates the crystalline nature of the Si nanostructure. However, only Bragg-oriented Si nanocrystals are visible, hence the crystalline fraction is underestimated. In addition only Si nanocrystals larger than a minimum size are visible; as a consequence, it becomes difficult to observe the crystallinity of the smaller Si structures at the SRO-substrate interface region [37].

#194332 - $15.00 USD Received 22 Jul 2013; revised 20 Sep 2013; accepted 24 Sep 2013; published 4 Oct 2013

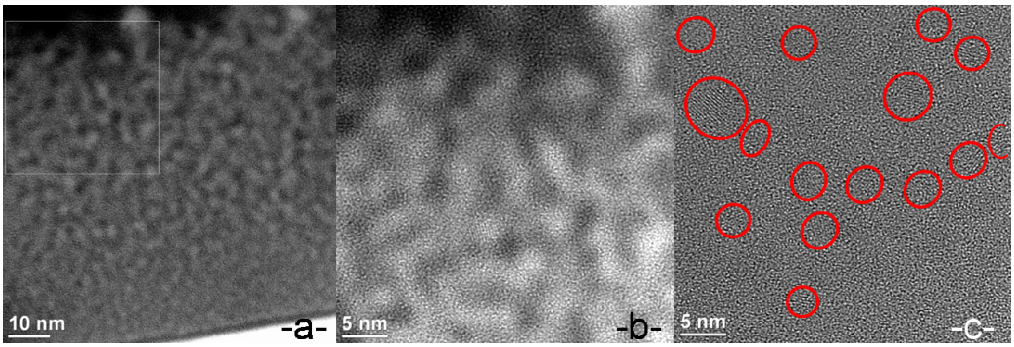

Fig. 4. a) Cross-sectional Si plasmon EFTEM image of the SRO-substrate interface region of the laser-annealed area recorded at an energy loss of E_{loss} = 17 eV with an energy slit width of 5 eV, b) magnified Si plasmon EFTEM image of the area marked in a), c) cross-sectional zero-loss filtered HRTEM image of the same field of view as in b).

4. Conclusions

Using energy-filtered TEM it has been shown that we obtained percolated Si nanostructures by spontaneous self-structuring during spinodal decomposition of metastable Si-rich oxides under laser irradiation. These nanostructures (<5nm) are expected to show larger bandgaps due to the quantum confinement effect and can thus be utilized in a tandem PV cells allowing a better use of the solar spectrum. These percolated sponge-like structures embedded in and passivated by the oxide matrix should have the advantage of making efficient use of UV photons as well as overcoming the difficulty of carrier separation and charge transport.

Acknowledgments

We thank our colleagues from HZDR Dresden-Rossendorf, Dr. Bernd Schmidt and Mr. David Friedrich for valuable discussions, Ms. Annette Kunz and Ms. Elfi Christalle for TEM sample preparations with FIB and Dr. Jan Lehmann for ERD analysis. This work is supported by BMBF (German)-TÜBITAK (Turkey) project Rainbow Energy (Grant no: 109R037).

#194332 - $15.00 USD Received 22 Jul 2013; revised 20 Sep 2013; accepted 24 Sep 2013; published 4 Oct 2013